OSCILLATING LIGHT WALL ABOVE A SUNSPOT LIGHT BRIDGE

Shuhong Yang¹, Jun Zhang¹, Fayu Jiang¹, and Yongyuan Xiang²

Accepted for publication in ApJL

ABSTRACT

With the high tempo-spatial Interface Region Imaging Spectrograph 1330 Å images, we find that many bright structures are rooted in the light bridge of NOAA 12192, forming a light wall. The light wall is brighter than the surrounding areas, and the wall top is much brighter than the wall body. The New Vacuum Solar Telescope $H\alpha$ and the Solar Dynamics Observatory 171 Å and 131 Å images are also used to study the light wall properties. In 1330 Å, 171 Å, and 131 Å, the top of the wall has a higher emission, while in the $H\alpha$ line, the wall top emission is very low. The wall body corresponds to bright areas in 1330 Å and dark areas in the other lines. The top of the light wall moves upward and downward successively, performing oscillations in height. The deprojected mean height, amplitude, oscillation velocity, and the dominant period are determined to be 3.6 Mm, 0.9 Mm, 15.4 km s⁻¹, and 3.9 min, respectively. We interpret the oscillations of the light wall as the leakage of p-modes from below the photosphere. The constant brightness enhancement of the wall top implies the existence of some kind of atmospheric heating, e.g., via the persistent small-scale reconnection or the magneto-acoustic waves. In another series of 1330 Å images, we find that the wall top in the upward motion phase is significantly brighter than in the downward phase. This kind of oscillations may be powered by the energy released due to intermittent impulsive magnetic reconnection.

Subject headings: sunspots — Sun: atmosphere — Sun: oscillations — Sun: UV radiation

1. INTRODUCTION

In the sunspot umbra, the overturning motion of the plasma is hindered by the strong magnetic field, thus leading to a lower temperature in the photosphere due to the reduced energy input (Gough & Tayler 1966). Within the umbra, light bridges (LBs) are one kind of bright structures with incompletely suppressed convection (Sobotka et al. 1993; Borrero & Ichimoto 2011). LBs are considered to have a deep anchoring in the convection zone (Lagg et al. 2014). Faint LBs penetrate into the umbra, and strong LBs can divide the umbra into separate umbral cores (Sobotka et al. 1994; Rimmele 2008). The widths of LBs mainly range from no more than one arcsecond to several arcseconds, and the typical brightness is comparable to the penumbra. In LBs, the magnetic field is weaker and the magnetic inclination is higher than in the neighboring umbra, forming a magnetic canopy (Lites et al. 1991; Rüedi et al. 1995; Leka 1997; Jurčák et al. 2006; Sobotka et al. 2013). The umbral cores separated by a LB have either the opposite or the same magnetic polarities (Zirin & Wang 1990; Sobotka et al. 1994).

Sunspot oscillations have been extensively observed and investigated for nearly half a century since their discovery (Beckers & Tallant 1969). The oscillation power in a sunspot is non-uniformly distributed. The oscillations with a period of about 3 min are prominent in the umbra and the 5-min oscillations dominate the penumbra (Christopoulou et al. 2000; Yuan et al. 2014a). In the umbra, 5-min oscillations are greatly suppressed (Zirin & Stein 1972; Stangalini et al. 2012). Umbral oscil-

² Fuxian Solar Observatory, Yunnan Observatories, Chinese Academy of Sciences, Kunming 650011, China

lations are explained as standing slow mode magnetoacoustic waves between the photosphere and transition region (Botha et al. 2011). The 3-min oscillations appear as slow magneto-acoustic waves propagating along the magnetic field lines from the umbra to the corona (de Moortel 2009; Kiddie et al. 2012; Tian et al. 2014; Cho et al. 2015). The running penumbral waves are observed to be disturbances propagating outward along the penumbra with the period around 300 s (Zirin & Stein 1972; Tziotziou et al. 2006). The oscillations in LBs have not been well studied until now. The atmosphere above LBs is often manifested in forms of brightnings, jets, and surges (Shimizu et al. 2009). Sobotka et al. (2013) analyzed the oscillations above a pore lacking a penumbra, and found that the power dominant in the LB is around 4 mHz, i.e., 4.2 min. Recently, Yuan et al. (2014b) studied the variations of LB intensity in solar active region (AR) 11836, and their results showed that 5-min oscillations are significantly presented in LBs and the 3-min oscillations in LBs are suppressed.

NOAA 12192 which occurred in the quite weak solar cycle 24 is the largest AR since 1990 November (Thalmann et al. 2015; Sun et al. 2015). During the passage of AR 12192 across the visible solar disk in 2014 October, the Interface Region Imaging Spectrograph (IRIS; De Pontieu et al. 2014) was operated to observe the AR with a field-of-view (FOV) of 119"×119" and obtained quite a lot of excellent data. Especially, a period of about 1 hr around 06:00 UT on October 25 was spent observing the light bridge dynamics as designed, and a series of high tempo-spatial images were obtained. In the present study, we report the discovery of oscillating light wall above a light bridge in AR 12192, using the jointed observations from the IRIS, the Solar Dynamics Observatory (SDO; Pesnell et al. 2012), and the New Vacuum Solar Telescope (NVST; Liu et al. 2014) of the Fuxian

¹ Key Laboratory of Solar Activity, National Astronomical Observatories, Chinese Academy of Sciences, Beijing 100012, China; shuhongyang@nao.cas.cn

Solar Observatory in China.

2. OBSERVATIONS AND DATA ANALYSIS

Two series of IRIS slit-jaw 1330 Å images (SJIs) are adopted. The 1330 Å passband contains emission from the strong C II 1334/1335 Å lines formed in the chromosphere and lower transition region, and also includes continuum emission formed around the temperature minimum (upper photosphere and lower chromosphere). On October 25, the SJIs in 1330 Å were taken from 05:17:13 UT to 06:30:18 UT with a spatial resolution of 0."166 $pixel^{-1}$ and a cadence of 7 s. On October 29, the 1330 Å SJIs were obtained from 15:30:00 UT to 18:17:49 UT with a cadence of 16 s and a pixel size of 0."333. The NVST was also pointed to AR 12192 on October 25, and two series of H α and TiO images were obtained. The H α 6562.8 Å observations were from 04:59:20 UT to 05:59:15UT with a cadence of 12 s, and have a FOV of 152" \times 152" with a spatial sampling of 0".164 pixel⁻¹. We also use one TiO 7058 Å image taken at 05:50:03 UT with a pixel size of 0."052 to show the AR appearance. The Level 0 H α and TiO images are firstly calibrated to Level 1 including dark current subtraction and flat field correction, and then the Level 1 images are further reconstructed to Level 1+ by speckle masking (see Weigelt 1977; Lohmann et al. 1983).

Moreover, we also use the Helioseismic and Magnetic Imager (HMI; Scherrer et al. 2012; Schou et al. 2012) and the Atmospheric Imaging Assembly (AIA; Lemen et al. 2012) observations from the SDO during the IRIS observational periods. We use the full-disk HMI line-of-sight magnetograms with a spatial sampling of 0''.5 pixel⁻¹ and a cadence of 45 s. The AIA monitors the Sun with a pixel size of 0''.6 and a cadence of 12 s. Here, the AIA 171 Å and 131 Å images are chosen to study the light wall at different temperatures. Then, we co-align all the IRIS, NVST, and SDO images with the cross-correlation method according to specific features (Yang et al. 2015).

3. RESULTS

The overview of AR 12192 on October 25 is displayed in Figure 1(a). The polarities of the leading and following sunspots are positive and negative, respectively. In the following sunspot, there is a weak magnetic field channel in the strong fields (outlined by the white square). The FOV outlined by the white square in panel (a) is partially covered by NVST TiO observations. The TiO image (panel (b)) which is rotated 135° anticlockwise shows the fine structures of the umbra and penumbra. There is a distinct strong light bridge (denoted by the arrow) crossing the umbra. The width of the photospheric light bridge distinguished in the TiO image is about 3'' (2.2) Mm). The corresponding IRIS 1330 Å image is displayed in panel (c). In the 1330 Å image, many bright structures are rooted in the light bridge, forming a light wall (denoted by the arrow). To view the light wall well, the expanded image outlined by the rectangle is shown in panel (d). The light wall is brighter compared with the surrounding areas. Especially, the top and base (indicated by the arrows) of the wall are brighter than the wall body.

3.1. Multi-wavelength appearance of the light wall

We use the multi-wavelength observations to study the properties of the light wall in detail. The NVST $H\alpha$, SJI 1330 Å, AIA 171 Å, and 131 Å images around 05:50 UT on October 25 are shown in Figures 2(a)-(d), respectively, and the FOV is outlined by the square in Figure 1(d). In the 1330 Å image in Figure 2(b), there is a bubblelike structure (delineated by the black curve) between the top (upper bright structure) and base (lower bright structure) of the light wall. We can see that the bubble also corresponds to a dark region in $H\alpha$ (panel (a)), 171 Å (panel (c)), and 131 Å (panel (d)) images. The top of the light wall appears as a bright structure in 171 Å and 131 Å images, while it could not be identified in the $H\alpha$ image. On the contrary, the base of the light wall appears as a bright structure in H α and 1330 Å, which cannot be found in 171 Å and 131 Å images.

We make the multi-wavelength cuts along slice "A-B" (see the white line in Figure 2(b)) and present them in Figure 2(e). The deep, light, and deep pink shadows from left to right mark the locations of the base, body, and top of the light wall, respectively. In the H α cut (the green curve), the high emission corresponds to the wall base location. The further the location away from the base is, the lower the $H\alpha$ emission is. In the 1330 Å cut (the dark curve), there are two peaks. The larger one (marked with the cross symbol) corresponds to the top of the light wall, and the smaller peak corresponds to the wall base. The emission of the wall body is lower than those of the wall top and base, however, it is higher than that of the nearby area (see the dashed line). In the 171 Å cut (the red curve), the high emission is at the wall top location, and the emissions at the foot and body locations are quite low.

3.2. Oscillations of the light wall

Figures 3(a1)-(a5) display the evolution of the light wall which is outlined by the rectangle in Figure 2(b). We can see that the wall top rose first and then fell down. From 05:49:04 UT to 05:51:52 UT, the projected height of the wall increased by 0.8 Mm in about 3 min. Then it decreased by 0.4 Mm in the following 1.5 min. Along slice "C-D" marked in Figure 3(a5), we make a space-time plot, which is displayed in panel (b). The most conspicuous behavior revealed by the plot is that there exists continuous oscillations of the bright top of the light wall. The solid blue curve outlines the position evolution of the wall top, and the dashed line marks the base of the light wall. The distance between the wall base and the wall top is calculated as the height of the light wall. It should be noted that, in order to reduce the effect of the wall width on the wall height, the wall height h is measured from the base center to the top center. The mean projected wall height is $\overline{h} = \frac{\sum_{0}^{n-1} h_i}{n}$, where h_i is the projected height in frame i. The mean projected amplitude of oscillations is $\overline{amp} = \frac{\sum_{0}^{n-1} |\Delta H_j/2|}{N}$, and the mean projected oscillations is $\overline{amp} = \frac{\sum_{0}^{n-1} |\Delta H_j/2|}{N}$. tion velocity is $\overline{v} = \frac{\sum_{0}^{N-1} |\Delta H_{j}/\Delta T_{j}|}{N}$, where ΔH_{j} and ΔT_{j} are the height difference and time difference between the neighboring peak and valley, respectively. The heliocentric angle (α) of the light wall is 26°. When considering the projection effect, the corrected mean height of the

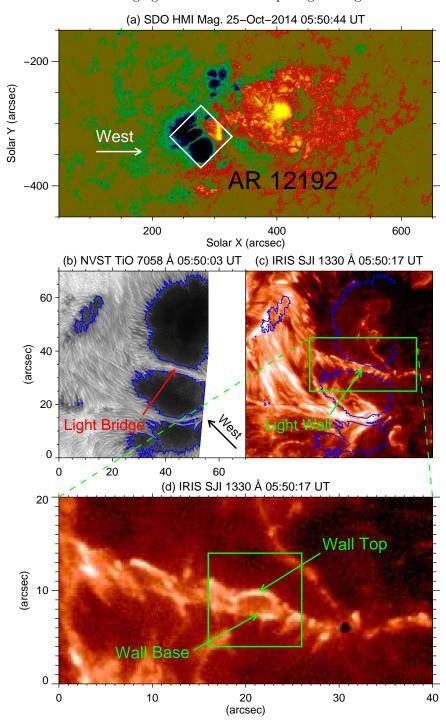


Fig. 1.— Panel (a): SDO HMI line-of-sight magnetogram displaying the overview of AR 12192. Panels (b)-(c): NVST TiO 7058 Å and IRIS SJI 1330 Å images (also see animation 1) showing the light bridge and the light wall in the FOV outlined by the square in panel (a). The blue curves in panels (b) and (c) are the contours of the sunspot umbra. Panel (d): expanded view of the 1330 Å image outlined by the rectangle in panel (c). The square outlines the FOV of Figures 2(a)-(d).

wall is \overline{ht} . = $\overline{h}/\sin\alpha$ = 3.6 Mm, the mean amplitude is $\overline{AMP} = \overline{amp}/\sin\alpha = 0.9$ Mm, and the mean oscillation velocity is \overline{vel} . = $\overline{v}/\sin\alpha = 15.4$ km s⁻¹. We apply the Morlet wavelet method to the heights of the light wall, and show the wavelet power spectrum in panel (c). It clearly reveals that there is a main oscillation period around 4 min. The global power (see panel (d)) shows that the main period is 3.9 min.

On 2014 October 29, AR 12192 moved to a location close to the west limb (Figure 4(a)). The light wall oscillated continually, and some part of the wall top performed an interesting behavior, i.e., the wall top was brighter in the upward motion phase than in the downward phase. To describe this kind of performance well, a section of the light wall (outlined by the rectangle in panel (a)) is focused on. A series of sub-region images are displayed in panels (b1)-(b5). At 16:34:02 UT, the top

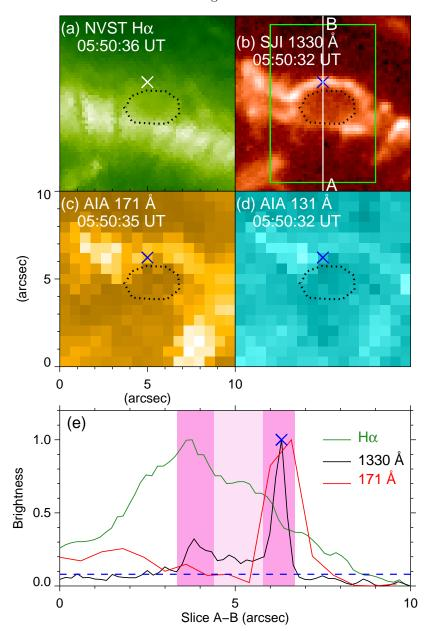


Fig. 2.— Panels (a)-(d): NVST H α , SJI 1330 Å, AIA 171 Å and 131 Å images showing the appearance of the light wall at different temperatures. The dotted curves delineate the general shape of a bubble-like structure identified in the 1330 Å image. The rectangle in panel (b) outlines the FOV of Figures 3(a1)-(a5). Panel (e): multi-wavelength brightness along slice "A-B" marked in panel (b). The deep, light, and deep pink shadows mark the wall base, wall body, and wall top, respectively.

of the wall appeared as a bright structure, as labeled between the parallel lines in panel (b1). One minute later, the bright structure moved upward to a higher position and became much brighter (see panel (b2)). The bright structure then reached to the highest position, and its emission became weaker (see panel (b3)). After that, the wall top moved downward with a weak emission (panels (b4)-(b5)).

To further study the evolution of the light wall, we make a space-time plot along slice "E-F" marked in Figure 4(b2), and present it in Figure 5(a). The blue curve in Figure 5(a) outlines the evolution of the wall top. The wall top performed oscillations with the average period of about 4.5 min. The red asterisks mark the locations of the maxima and the minima of four periods. The vertical

dashed lines separate the different periods. The heliocentric angle of the light wall is 78°. Then the deprojected mean height of the wall is about 3.8 Mm, the mean amplitude is 1.0 Mm, and the mean oscillation velocity is 14.4 km s⁻¹. These values are consistent with those obtained using the October 25 series. Especially, the deprojected wall heights obtained at different times are comparable, implying that the wall width does not significantly affect the height measurement of the light wall. It seems that, for each period, the emission of the wall top in the upward motion stage is higher than in the downward motion stage. To quantitatively study this property, the brightness of the wall top is plotted with the blue curve in panel (b). In addition, the green curve in panel (b) is the brightness of the wall body (along the green line

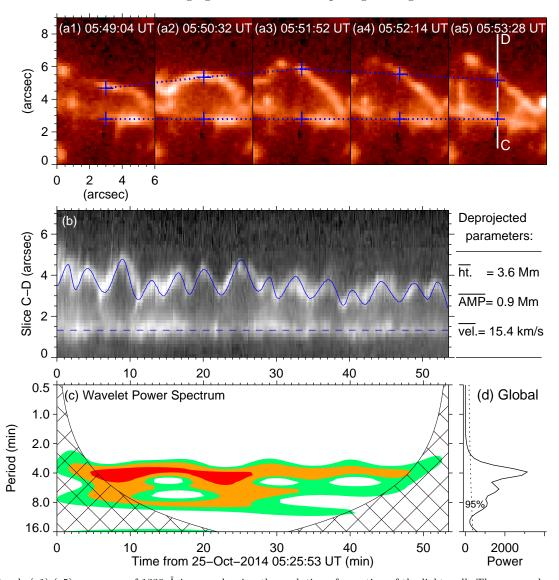


Fig. 3.— Panels (a1)-(a5): sequence of 1330 Å images showing the evolution of a section of the light wall. The upper plus symbols and the lower ones mark the top and base of the wall at different times. Panel (b): space-time plot along slice "C-D" marked in panel (a5). The solid curve delineates the wall top, and the dashed line marks the wall base. Panels (c) and (d): wavelet power spectrum and the global power of the light wall oscillations.

in panel (a)). The mean brightness of the wall body is about 4 I_0 , where I_0 is the umbra brightness in 1330 Å. We can see that the brightness of the wall top is higher than the wall body all the time. The mean brightness of the wall top is about 12 I_0 and that of the wall body is about 4 I_0 . The mean brightness values in the four downward motion stages (gray shadow regions) are 9.3 I_0 , 8.1 I_0 , 5.9 I_0 , and 6.0 I_0 , smaller than those (16.5 I_0 , 21.1 I_0 , 11.2 I_0 , and 10.5 I_0) in the upward stages (white regions), respectively.

4. CONCLUSIONS AND DISCUSSION

With the high tempo-spatial *IRIS* 1330 Å observations, we find an ensemble of oscillating bright features in the chromosphere and transition region above a light bridge, and name this ensemble with a new term *light wall*. The light wall is brighter than the surrounding regions, and the top and base of the light wall are much brighter than the wall body. In addition, we use the NVST and AIA multi-wavelength data to study the prop-

erties of the light wall. We find that the wall top appeared as a similar bright structure in 1330 Å, 171 Å, and 131 Å images while it can not be identified in the H α line. The wall body appeared as a bright structure in 1330 Å and as a dark structure in the other lines. The wall top moved upward and downward successively, performing continuous oscillations. The deprojected average height, amplitude, and oscillation velocity are about 3.6 Mm, 0.9 Mm, and 15.4 km s $^{-1}$, respectively. By applying the wavelet analysis method to the heights of the light wall, we find that the main oscillation period is 3.9 min. In another series of IRIS 1330 Å images, we find that the wall top in the upward motion phase was brighter than in the downward phase.

The previous studies (Sobotka et al. 2013; Yuan et al. 2014b) about LB oscillations were done through examining the intensity variations or the Doppler characters in LBs. In the present paper, we find a dynamical light wall rooted in the LB, and have directly observed the

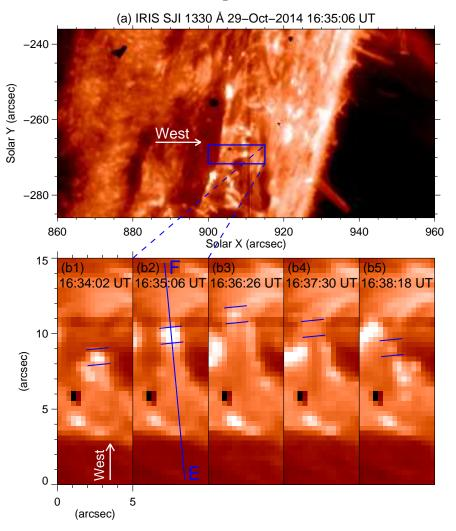


Fig. 4.— Panel (a): IRIS 1330 Å image showing the light wall on October 29 (also see animation 2). Panels (b1)-(b5): 1330 Å images at different times showing the evolution of a section of the light wall outlined by the rectangle in panel (a). Two short parallel lines in each panel mark the wall top, and line "E-F" in panel (b2) marks the position along which the space-time plot shown in Figure 5(a) is obtained.

light wall oscillations in height for the first time. The dominant period of the light wall oscillations is 3.9 min, comparable with that (4.2 min) determined by Sobotka et al. (2013). We interpret the oscillations of the light wall as the leakage of p-modes from below the photosphere. The p-modes are global resonant acoustic oscillations appearing as photospheric velocity and intensity pulsations. The p-modes can leak enough energy to drive upward flows (De Pontieu et al. 2004), resulting in the oscillations of the light wall.

Over the light bridge in NOAA AR 10132, Berger & Berdyugina (2003) observed persistent brightness enhancement in the 1600 Å images from the *Transition Region and Coronal Explorer* (*TRACE*) satellite. They interpreted the enhanced LB brightness in 1600 Å as magnetic heating through some kind of magnetic reconnection which is still unclear. According to Klimchuk (2006), oscillations can carry acoustic flux, a significant energy flux, to higher atmosphere to heat the solar atmosphere. Moreover, in a study of the LB in NOAA 11005, Sobotka et al. (2013) measured the acoustic power flux leaking along the magnetic fields in the LB from the photosphere to the chromosphere, and found that the transferred en-

ergy flux is sufficient to balance the total radiative losses of the LB in the chromosphere. In the present study, for the light wall on October 25, the wall top appeared as a constant enhancement in brightness, which can be observed in 1330 Å, 171 Å, and 131 Å lines, implying that there exists some kind of atmospheric heating. However, it is difficult to know which one is the exact mechanism for the wall top heating: the persistent small-scale reconnection or the magneto-acoustic waves. For the light wall on October 29, the wall top was significantly brighter in the upward motion stage than in the downward phase, implying that there was an intermittent heating during each oscillation period. We suggest that this kind of dynamical behavior may be powered by the energy released due to intermittent impulsive magnetic reconnection.

We thank the referee for his/her valuable suggestions. This work is supported by the National Natural Science Foundations of China (11203037, 11221063, 11303049, and 11373004), the CAS Project KJCX2-EW-T07, the National Basic Research Program of China under grant 2011CB811403, and the Strategic Priority Research Program—The Emergence of Cosmologi-

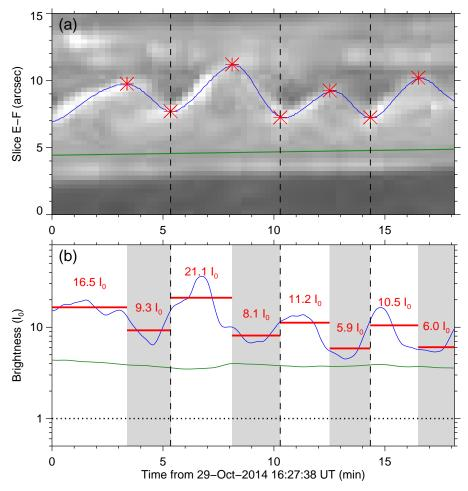


Fig. 5.— Panel (a): space-time plot derived along slice "E-F" marked in Figure 4(b2). The blue curve outlines the top of the light wall. The red asterisks mark the locations of the maxima and the minima of four periods which are separated by three vertical dashed lines. Panel (b): brightness of the wall top (blue curve) and wall body (green curve) along the blue curve and green line in panel (a). The dotted line is the brightness of the umbra. The white and gray regions mark the upward and downward motion stages, respectively. The red lines associated with labels indicate the average brightness in different stages.

cal Structures of the Chinese Academy of Sciences (No. XDB09000000). The data are used by courtesy of IRIS, NVST, and SDO science teams. IRIS is a NASA small explorer mission developed and operated by LMSAL with

mission operations executed at NASA Ames Research center and major contributions to downlink communications funded by the Norwegian Space Center (NSC, Norway) through an ESA PRODEX contract.

REFERENCES

Beckers, J. M., & Tallant, P. E. 1969, Sol. Phys., 7, 351 Berger, T. E., & Berdyugina, S. V. 2003, ApJ, 589, L117 Borrero, J. M., & Ichimoto, K. 2011, Living Reviews in Solar Physics, 8, 4

Botha, G. J. J., Arber, T. D., Nakariakov, V. M., & Zhugzhda, Y. D. 2011, ApJ, 728, 84

Cho, K.-S., Bong, S.-C., Nakariakov, V. M., et al. 2015, ApJ, 802, 45

Christopoulou, E. B., Georgakilas, A. A., & Koutchmy, S. 2000, A&A, 354, 305

de Moortel, I. 2009, Space Sci. Rev., 149, 65

De Pontieu, B., Erdélyi, R., & James, S. P. 2004, Nature, 430, 536
 De Pontieu, B., Title, A. M., Lemen, J. R., et al. 2014, Sol. Phys., 289, 2733

Gough, D. O., & Tayler, R. J. 1966, MNRAS, 133, 85

Jurčák, J., Martínez Pillet, V., & Sobotka, M. 2006, A&A, 453, 1079

Kiddie, G., De Moortel, I., Del Zanna, G., McIntosh, S. W., & Whittaker, I. 2012, Sol. Phys., 279, 427

Klimchuk, J. A. 2006, Sol. Phys., 234, 41

Lagg, A., Solanki, S. K., van Noort, M., & Danilovic, S. 2014, A&A, 568, A60 Leka, K. D. 1997, ApJ, 484, 900

Lemen, J. R., Title, A. M., Akin, D. J., et al. 2012, Sol. Phys., 275, 17

Lites, B. W., Bida, T. A., Johannesson, A., & Scharmer, G. B. 1991, ApJ, 373, 683

Liu, Z., Xu, J., Gu, B.-Z., et al. 2014, Research in Astronomy and

Astrophysics, 14, 705
Pesnell, W. D., Thompson, B. J., & Chamberlin, P. C. 2012, Sol. Phys., 275, 3

Rimmele, T. 2008, ApJ, 672, 684

Rüedi, I., Solanki, S. K., & Livingston, W. 1995, A&A, 302, 543
Scherrer, P. H., Schou, J., Bush, R. I., et al. 2012, Sol. Phys., 275, 207

Schou, J., Scherrer, P. H., Bush, R. I., et al. 2012, Sol. Phys., 275, 229

Shimizu, T., Katsukawa, Y., Kubo, M., et al. 2009, ApJ, 696, L66 Sobotka, M., Bonet, J. A., & Vazquez, M. 1993, ApJ, 415, 832 Sobotka, M., Bonet, J. A., & Vazquez, M. 1994, ApJ, 426, 404 Sobotka, M., Švanda, M., Jurčák, J., et al. 2013, A&A, 560, A84 Stangalini, M., Giannattasio, F., Del Moro, D., & Berrilli, F.

2012, A&A, 539, L4

Sun, X., Bobra, M. G., Hoeksema, J. T., et al. 2015, arXiv:1502.06950

Thalmann, J. K., Su, Y., Temmer, M., & Veronig, A. M. 2015, ApJ, 801, L23

Tian, H., DeLuca, E., Reeves, K. K., et al. 2014, ApJ, 786, 137 Tziotziou, K., Tsiropoula, G., Mein, N., & Mein, P. 2006, A&A,

Weigelt, G. P. 1977, Optics Communications, 21, 55 Yang, S., Zhang, J., & Xiang, Y. 2015, ApJ, 798, L11 Zirin, H., & Wang, H. 1990, Sol. Phys., 125, 45

Zirin, H., & Stein, A. 1972, ApJ, 178, L85

A&A, 561, A19

41

Yuan, D., Sych, R., Reznikova, V. E., & Nakariakov, V. M. 2014a,

Yuan, D., Nakariakov, V. M., Huang, Z., et al. 2014b, ApJ, 792,